International Journal of Industrial Engineering, 29(6), 893-913, 2022

ENERGY MANAGEMENT AND HARMONIC MITIGATION OF HYBRID RENEWABLE ENERGY MICROGRID USING COORDINATED CONTROL OF MULTI-AGENT SYSTEM

Loganathan Navaneetha Krishnan[1, *], Mayurappriyan Pudupalayam Sachithanandam[2], and Lakshmi Kaliappan[3]

[1]Department of Electrical and Electronics Engineering
Sri Krishna College of Engineering and Technology
Tamilnadu, India
[*]Corresponding author's e-mail: loganathann@skcet.ac.in

[2]Department of Electronics and Instrumentation Engineering
Kumaraguru College of Technology
Tamilnadu, India

[3]Department of Electrical and Electronics Engineering
K.S.R. College of Engineering
Tamilnadu, India

In this paper, a novel energy management method that is based on a Multi-Agent System (MAS) is presented for hybrid Distributed Energy Sources (DES) in a microgrid. These DESs include Photovoltaic (PV), wind energy systems, and Fuel Cell (FC) in the Microgrid (MG). The MG is responsible for supplying both active and reactive powers, allowing it to serve variable linear and non-linear loads. The MAS that has been proposed and is based on a decentralized control structure offers control not only for the energy management of the Distributed Generation (DG) but also for the management of power flow between the MG and the power grid that is connected to the MG. This control is offered by the MAS. The main objective of the control strategy is to manage the amount of energy that is transferred between the power grid and the MG concerning the supply conditions of the required internal energy via DES, which will ultimately result in a reduction in the dependence on the MG on the grid. For current harmonic compensation, a Static Compensator (STATCOM) with a Fuzzy Logic (FL) based Instantaneous Reactive Power control scheme is used. On the other hand, a discrete controller is utilized to manage the energy of the MG. The findings of the simulation and the experiments demonstrated that the implementation of the suggested Energy Management System (EMS) has good performance as a novel energy management solution for a hybrid distributed power generating system and harmonic compensation.

Keywords: Hybrid Renewable Energy Sources; Power Quality; Energy Management; Fuzzy Logic Controller; Multi-Agent System.

(Received on July 9, 2022; Accepted on October 6, 2022)

1. INTRODUCTION

An MG is made up of several DG sources and energy storage units all working together. A microgrid is a set of energy generators that can supply the energy required for a load through a decentralized system in both standalone and grid-connected modes. These energy generators include wind energy, solar photovoltaic arrays, Battery Energy Storage Systems (BESS), and FC (Dash and Bajpai, 2015; Shahgholian, 2021; Rajesh *et al.*, 2017). The integration of Renewable Energy Sources (RES) like solar and wind power, which have limited programmability and predictability, into power grids has made it feasible to reap the advantages of renewable energy sources. This was made possible by the completely programmable combination of RES. The use of an FC as a backup source for an MG, in addition to PV and wind energy systems, results in an increased level of operational reliability. When employing MGs, however, it is vital to keep in mind the Energy Management System (EMS), compensating for power shortages by FCs, and maintaining the balance between output and consumption in both stand-alone and grid-connected modes (Tseng *et al.*, 2014; Toghani *et al.*, 2020).

Research on MG has progressed quite a bit up to this point. Power electronic controllers in MGs are the subject of some latest research. There is a dependable controller for micro-turbines and electrolyzers that are used in MGs for

frequency regulation that can be found in the reference. Regarding the issue of power fluctuations in an MG, a fuzzy logic Proportional-Integral-Derivative (PID) controller is presented to regulate the electrolyzer (Ngamroo, 2012). This approach is offered as a possible solution. On the other hand, the modeling of equipment has been largely ignored in the majority of the studies that have been published in the area of management and control strategy of MGs; instead, the emphasis has been placed on providing a management approach. The majority of MG's energy management systems, as well as their methods, are formed on the basis of a centralized structure (Mohammed *et al.*, 2019; Wang *et al.*, 2015). However, due to increased communication and telecommunication costs, the use of centralized control and management methods is no longer cost-effective. This is because of the rapid growth of MGs in power grids as well as the increase in the number of MGs, as well as the presence of generators and various types of loads (Karavas *et al.*, 2015).

Along with any alteration to the power network, centralized control systems need to have their structures reorganized, and their software brought up to date. MGs are superior in terms of robustness, cost-effectiveness, and simplicity in terms of energy regulation and management. This is because MASs are designed based on decentralized structures (Wang *et al.*, 2014; Dou *et al.*, 2015). As a result, the majority of MG energy management control approaches have converged with multi-agent distributed systems over the last several years. According to the source, the management of the MG is suggested to be controlled by a hierarchical system consisting of three layers: a supervisory layer, an optimizing layer, and an execution layer. To control an MG via PVs, wind systems, and batteries, two controllers that are meant to function as master and slave are used (Benlahbib *et al.*, 2020; Xu *et al.*, 2015).

In electronic control systems, intelligent approaches like genetic algorithms, Particle Swarm Optimization (PSO) algorithms, and Fuzzy Logic Controllers (FLC) have also been applied. For instance, the genetic algorithm is used in reference to manage production in an MG that consists of a variety of different kinds of energy sources (Rahmani-Andebili, 2017). In addition, FLC is used in the process of optimizing the performance of MG generators. When non-linear loads are linked to a grid, this may produce disruptions in the voltage and current characteristics of the grid, which in turn can have a significant impact on MGs that are connected to the grid (Zeng *et al.*, 2013). Harmonic distortions are an example of one of the issues that might arise as a result of a non-linear load being applied to MGs. In recent years, several different approaches to harmonic correction have been utilized. The use of multi-agent and hierarchical systems is one of the ways that are not only effective but also feasible for harmonic compensation. In the majority of studies that have been conducted on the subject of MG management and control strategy, the primary emphasis has been on providing management strategy, while modeling and the dynamic behavior of MG devices and equipment have received much less attention (Talapur *et al.*, 2018). However, in order to manage and control energy in an MG, it is required to examine all sections of the MG, taking into consideration the dynamic and physical properties of the generators and power converters. Only then can energy be managed and controlled. As a result, the study demonstrates that the energy management and control of MG have been carried out with an adequate level of precision regarding the behaviors as well as the dynamic and physical features of the apparatus (Chauhan *et al.*, 2018).

Further realistic modeling of an MG has been used to explore the control approach that has been implemented. The modeling of photovoltaic systems, wind energy systems, and fuel cells all made use of dynamic details in addition to dynamic models for the DC-DC and DC-AC converters. In addition, converter capacity is one of the essential concerns that must be considered while managing the energy of MGs (Vijayakumar and Vijayan, 2014). Because the presence of harmonic loads in real power networks leads to the occupation of convertors' capacities, the energy management of an MG can mislead the issue in a direction that is different from reality if it does not take into consideration the limitations that are caused by the harmonic (Prasad et al., 2022; Prince *et al.*, 2019).

As a consequence of this, the issue of harmonic compensation with a non-linear harmonic load is added to the problem of energy management in this work to facilitate a more realistic simulation of an MG (Ambia *et al.*, 2014). In this discussion, the problem of developing an energy control strategy was approached from both a discrete and a continuous point of view. The suggested MAS has been successful in coordinating the continuous and discrete dynamics of the system, which is necessary for the effective energy management of the MG (Elgamal *et al.* 2020). This study focuses on the application of MAS to a hybrid renewable energy system to enhance its overall performance and efficiency. PV systems, wind turbines, and fuel cells make up the various components of the hybrid renewable energy system. The microgrid will be able to benefit from the implementation of the following solutions owing to the MAS-based EMS that has been proposed. A system for coordinating activities and a communication protocol that applies to all components of the microgrid. Control methods are based on the output characteristics of a variety of different kinds of power sources. Optimization of the functioning of the microgrid system, taking into consideration the load demand and the intermittent nature of renewable energy resources with improved power quality.

The following is the order in which the remaining portions of this paper are presented: 1. The proposed structure for an AC MG is described in Section 2. Hybrid Renewable Energy Source (HRES) -based STATCOM and Controller for HRES-based STATCOM are covered in Section 3. The use of MAS in the microgrid is shown in Section 4, along with the agent model for each component, MAS architecture, and controller for the EMS agent. In the meanwhile, a discussion of

the simulation and experimental findings of this work, which includes a case study and performance assessments conducted via a different situation, may be found in Section 5. The conclusions of this paper are discussed in Section 6, which is the last section.

2. PROPOSED STRUCTURE FOR AN AC MG

The topology of the power network that is presented in this article is comprised of an MG that integrates RES with PV, wind energy system, and FC. The proposed network has a load attached to it that is a mix of a changeable linear load and a non-linear load (Torreglosa et al., 2015). Additionally, the nonlinear load of the harmonic spectrum is the most intense of the 5th and 7^{th}-order harmonics, as illustrated in Figure 1. After DC-DC and DC-AC converters, the DES distributes its energy to customers at their Point of Common Coupling (PCC). On the one hand, the PCC's MG is linked to the grid as well. The presence of a non-linear harmonic load in the network necessitates the following: the energy required by the consumer as well as harmonic compensation should be provided internally by DES in the MG; additionally, the grid should not have permanent interference in the process of providing active and reactive power to the network. The FCs, on the other hand, serve as a backup source in the MG in general. However, this function is only activated if other generators are unable to provide the necessary amount of energy to the network. When this occurs, the FCs enter the circuit as backup energy sources and provide the necessary amount of energy. As a result, the proposed network requires an Energy Management Control System (EMCS) to make the most of the DES's full capacity, properly regulate the supply of energy to meet the requirements of consumers and compensates for network harmonics.

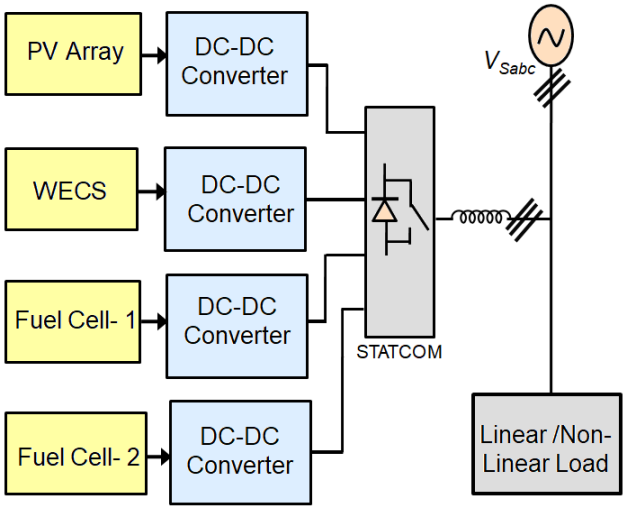

Figure 1. Proposed Structure of an AC MG

To investigate the functionality of these kinds of systems, one of the most important things to do is to create an accurate model of the behavioral dynamics of an electrical power production system. Three-phase thyristor rectifier used as a non-linear load: 3mH,5.7mH,12Ω, RL load used as a linear load: 7Ω,75mH. As a consequence of this, a detailed examination of the performance of a hybrid power production system requires careful modeling of photovoltaic systems, wind energy systems, and fuel cells. Additionally, the electronic power devices and equipment that are used inside the system need to be represented in an appropriate and precise manner. The development of a control system for the network that was examined is only possible with the assistance of this form of modeling.

3. HYBRID RENEWABLE ENERGY SOURCE BASED STATCOM

Figure 2 illustrates the Hybrid Renewable Energy Source (HRES) based STATCOM. STATCOMs attenuate harmonics by injecting active power with the same frequency but with a reverse phase to cancel that harmonic in MGs. This is done in conjunction with a 3-phase DC-AC Voltage Source Converter (VSC), which is utilized for the purpose of providing harmonic compensation. The reference current on the DQ frame is obtained by using the DQ axis with Fourier (DQF). The voltages V_{ia}, V_{ib}, and V_{ic} are the three-phase AC voltages of the inverter output, while I_a, I_b, and I_c are the three-phase AC currents of the inverter output (Muduli *et al.*, 2014). The bus voltages of the AC grid are represented by the symbols Vsa,

Vsb, and Vsc, respectively. The following equation may be used to represent the dynamic model of a 3-phase VSC-STATCOM.

$$\frac{di_{fx}}{dt} = \frac{R_f}{L_f} i_{fx} + \frac{1}{L_f} (V_{fx} - V_{Lx}) \quad (1)$$

where x = {a, b, c}, R_f and L_f are the resistance and inductance of the STATCOM line reactors, respectively.

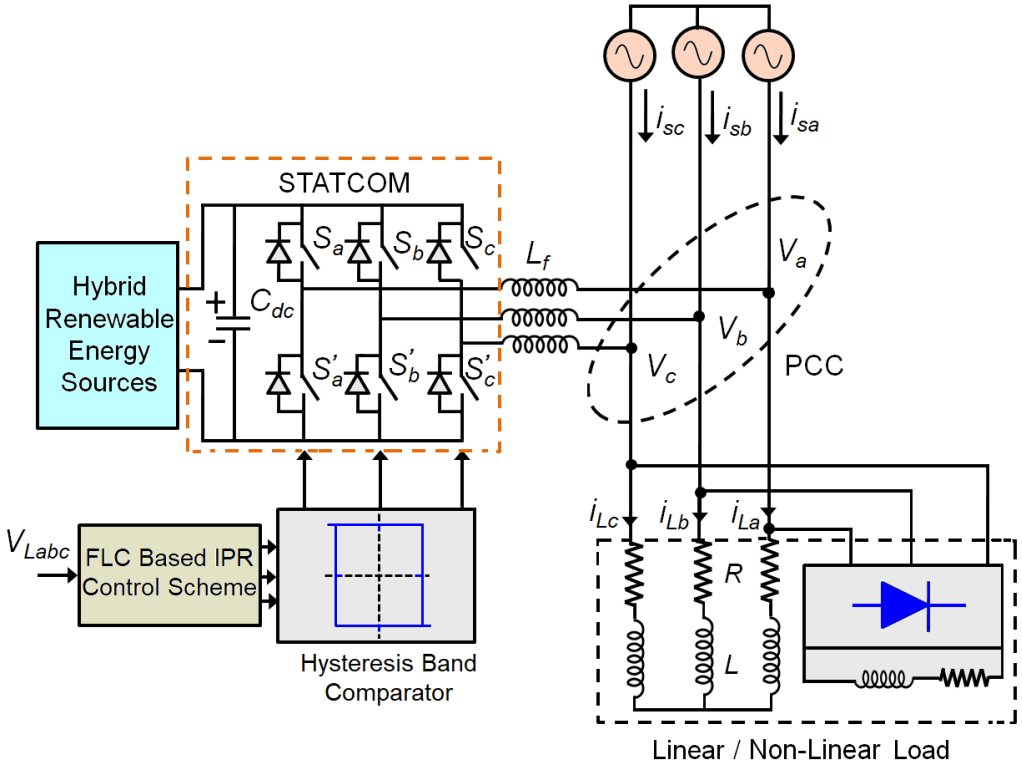

Figure 2. Hybrid Renewable Energy Source based STATCOM

The park transformation may be used to provide an expression for the voltage that is output by STATCOM.

$$V_{fd} = R_f\, i_d + L_f \frac{di_d}{dt} - L_f \omega\, i_q + V_{sd} \quad (2)$$

$$V_{fq} = R_f\, i_q + L_f \frac{di_q}{dt} + L_f \omega\, i_d + V_{sq} \quad (3)$$

The ω represents the angular velocities of the AC system, V_{id}, V_{iq}, I_d, and I_q stand for the voltages (V) and currents (A) that correspond to the *d* and *q* axes, respectively, and V_{sd} and V_{sq} are the bus voltages (V) of the AC grid.

3.1 Controller For HRES-based STATCOM

The schematic diagram for the current reference signals that are used by the FLC-based IPR control scheme is shown in Figure 3. By using the Clarke transformation and utilizing equations (4) and (5), the three-phase source voltages (Vsa, Vsb, and Vsc) are transformed into Vα,β coordinates (Muthuvel and Vijayakumar, 2020).

$$V_\alpha = \sqrt{\frac{2}{3}} \left[V_{sa} - \frac{V_{sb}}{2} - \frac{V_{sc}}{2} \right] \quad (4)$$

$$V\beta = \left[\frac{V_{sb} - V_{sc}}{\sqrt{2}} \right] \quad (5)$$

Similarly, the three-phase load currents (I_{La}, I_{Lb}, I_{Lc}) are detected and converted to $I_{0\alpha\beta}$ coordinates using Eqns. (6), (7), and (8).

$$I_0 = \sqrt{\frac{1}{3}}\,[I_{La} + I_{Lb} + I_{Lc}] \tag{6}$$

$$I_\alpha = \sqrt{\frac{2}{3}}\left[I_{La} - \frac{I_{Lb}}{2} - \frac{I_{Lc}}{2}\right] \tag{7}$$

$$I\beta = \left[\frac{I_{Lb} - I_{Lc}}{\sqrt{2}}\right] \tag{8}$$

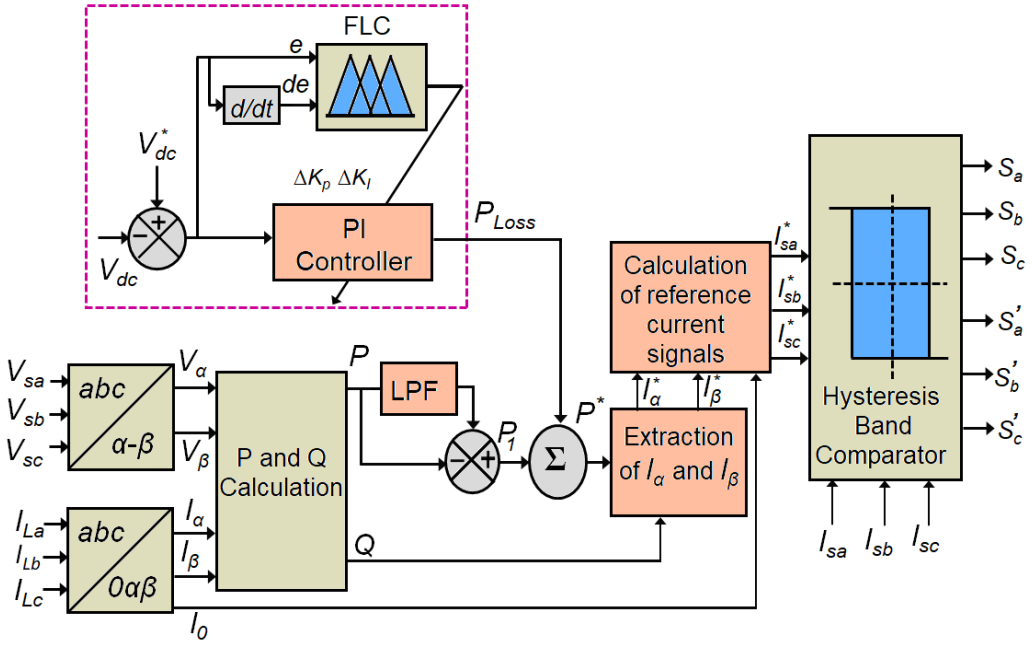

Figure 3. Schematic Diagram of the FLC-based IPR Control Scheme

The instantaneous active power (P) and reactive power (Q) are determined by using the Eqns. (9) and (10). After obtaining real power (P), it is divided into two categories: average real power and oscillating real power.

$$P = V_\alpha\, I_\alpha + V_\beta\, I_\beta \tag{9}$$

$$Q = V_\beta\, I_\alpha - V_\alpha\, I_\beta \tag{10}$$

The low pass filter is used to correct the harmonic active and reactive powers that are derived from *P (W)*. When P_1 and P_{Loss} are added together, the resulting value, P^*, represents the power flow that is required to keep the DC link voltage stable. After running the difference in error between the actual DC link voltage and the reference DC voltage through a PI controller, P_{Loss} may be computed and obtained.

$$P^* = P_1 + P_{Loss} \tag{11}$$

$$I_\alpha^* = \left[\left(\frac{-1}{V_\alpha^2 + V_\beta^2}\right)\left((P^* + V_\alpha) + (Q + V_\beta)\right)\right] \tag{12}$$

$$I_\beta^* = \left[\left(\frac{-1}{V_\alpha^2 + V_\beta^2}\right)\left((P^* \times V_\beta) - (Q + V_\alpha)\right)\right] \tag{13}$$

The Fuzzy Logic Controller (FLC) that is being used will create its control signal depending on the proportional and integral actions that are being performed by the PI controller (Delgoshaei *et al.*, 2021). The structure of the designed control is shown in Figure 3. The inputs to the controller are the error value (*e*), as well as the error derivative (*de*). The outputs of the fuzzy controller are denoted by the notations ΔK_p and ΔK_i, which stand for the proportional and integral actions of the PI controller, respectively. Negative (N), Zero (Z), and Positive (P) were the fuzzy set definitions that were assigned to the

input variables. On the other hand, five fuzzy set definitions were assigned to the output variables: Large Negative (LN), Small Negative (SN), Zero (Z), Small Positive (SP), and Large Positive (LP). The input and output membership functions are shown in Figures 4 and 5, respectively.

In the process of fuzzification, the min-max approach was used, and the defuzzification procedure was based on the maximum approach. Because the normalized quantities that were acquired have a crisp character, it is necessary to convert them to their equivalent fuzzy variables first. Following the process of fuzzification, the fuzzified inputs are sent to the fuzzy inference mechanism, which then, in accordance with the fuzzy rule base that has been provided, generates the normalized control output.

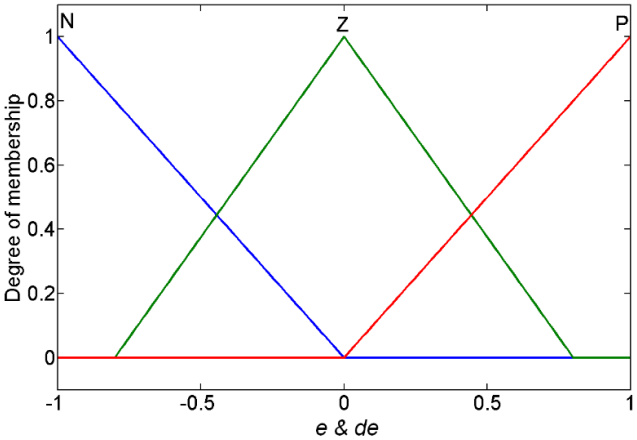

Figure 4. Membership Functions of the Error and its First Derivative

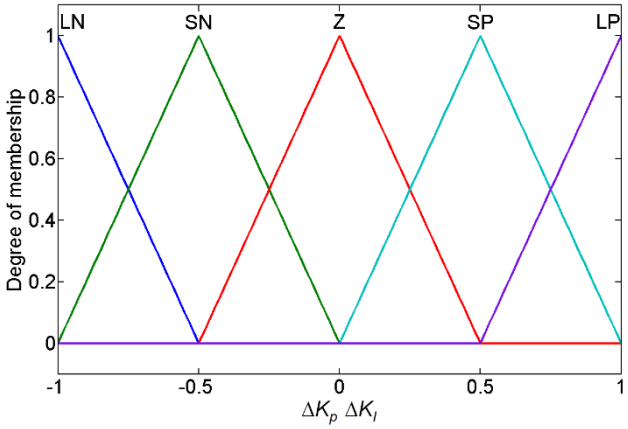

Figure 5. Membership Functions of the Outputs

The fuzzy rule base is shown in Table 1. Using the scaling factors, this output is changed such that it corresponds to the real control outputs Δ*K*p and Δ*K*i.

Table 1. Fuzzy Rule Base

de \ *e*	N	Z	P
N	LN	SN	Z
Z	SN	Z	SP
P	Z	SP	LP

We calculate the I^*_{abc} currents from P^* and Q, which, together with zero-sequence currents, are converted to reference currents by using inverse Clarke transformation as exposed in Eqns. (14), (15), and (16).

$$I_a^* = \sqrt{\frac{2}{3}}\left[I_\alpha^* + \frac{I_0}{\sqrt{2}}\right] \tag{14}$$

$$I_b^* = \sqrt{\frac{2}{3}}\left[\frac{-I_\alpha^*}{2} + \sqrt{\frac{2}{3}}\, I_\beta^* + \frac{I_0}{\sqrt{2}}\right] \tag{15}$$

$$I_c^* = \sqrt{\frac{2}{3}}\left[\frac{-I_\alpha^*}{2} - \sqrt{\frac{2}{3}}\, I_\beta^* + \frac{I_0}{\sqrt{2}}\right] \tag{16}$$

4. MAS STRUCTURE FOR MG ENERGY MANAGEMENT

The flexibility, adaptability, and independence of the MG have all been preserved via the use of an artificial intelligence-based MAS. The construction of MAS that is used to exert control over MG is shown in Figure 6.

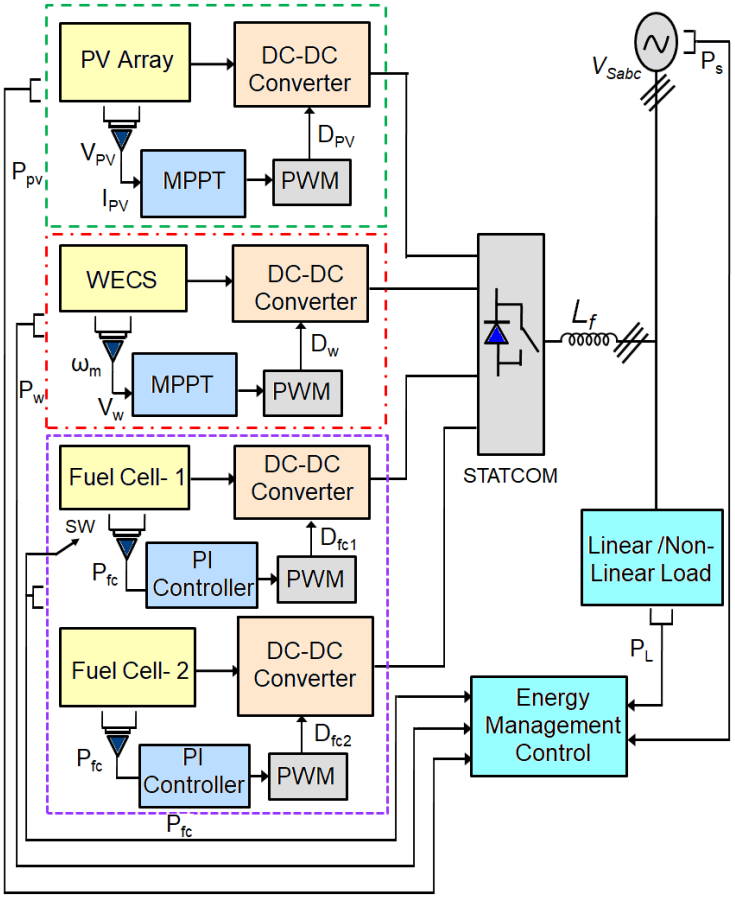

Figure 6. Schematic of Proposed MAS

The architecture of the system is such that it can provide the amount of electrical energy demanded by the fluctuating load while also taking into consideration the limits imposed by the surrounding environment and the system's changing conditions.

4.1 PV System Agent

An agent is responsible for representing the PV system. It will monitor the irradiance, as well as the performance of the PV system and the overall amount of electricity it generates. It is possible to see the PV system as an agent. This agent monitors the quantity of solar radiation that is received as well as the output power of the PV system to ensure that the PV system is functioning at its optimum level (Raja *et al.*, 2022; Parthiban and Vijayakumar, 2021). Figure 7 shows the PV system agent controller. This agent is fitted with an MPPT control unit, which enables optimal usage of the solar generator according to the amount of solar radiation. Control of the Maximum Power Point Tracker (MPPT) of the PV has been accomplished via the use of the Incremental Conductance (INC) approach. In the INC method, the current and voltage of the PV terminal is measured at regular intervals. After that, the amount of voltage is changed to achieve MPPT by comparing the increase in power to the increase in voltage or current between two consecutive samples. If there is a change in the operating voltage of the PV array and there is also an increase in the power, the system will modify the operating point of the PV array in that direction. If there is no change in any of these factors, the operating point will move in the other way. The benefit of using this approach is that it does not need previous knowledge of the characteristics of the PV panel. Additionally, it has excellent performance when there is not a significant shift in solar radiation over a short period.

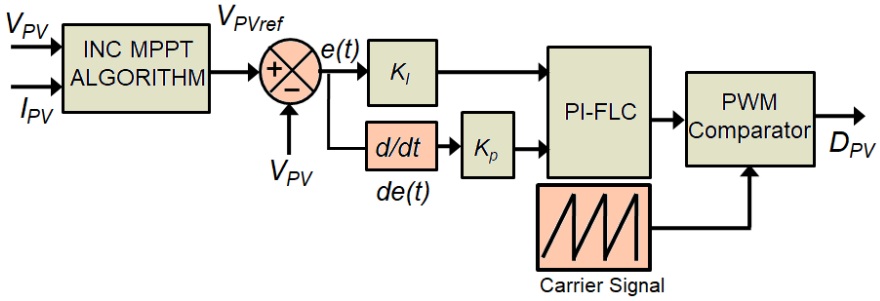

Figure 7. PV System Agent Controller

4.2 Wind Energy Conversion System Agent

An agent is responsible for representing the Wind Energy Conversion System (WECS). This agent will monitor the speed of the wind in addition to the overall performance of the wind turbines and the amount of electricity that they generate. Another element that contributes to the MAS is the wind system. Fig. 8 shows the WECS agent controller. This agent ensures that the operation is running as efficiently as possible by monitoring the wind speed and the power produced by WT. This agent is fitted with an MPPT controller unit, which enables the maximum functioning of the WT in accordance with the wind speed.

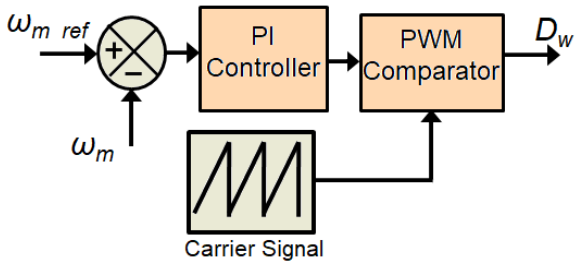

Figure 8. WECS Agent Controller

4.3 FC Agent

It is generally agreed that the FC system in MG acts as the third agent. This agent is responsible for monitoring the FCs' output power as well as their capacity for production, as well as the values of the factors that have an impact on that capacity. The energy management agent receives the necessary information from the FC agent to determine the power of the FCs. Because the primary responsibility of the FCs in the MG is to compensate for the lack of energy required by the network during power reductions caused by wind and solar generators, the control strategy for the FCs is depicted in Figure 9.

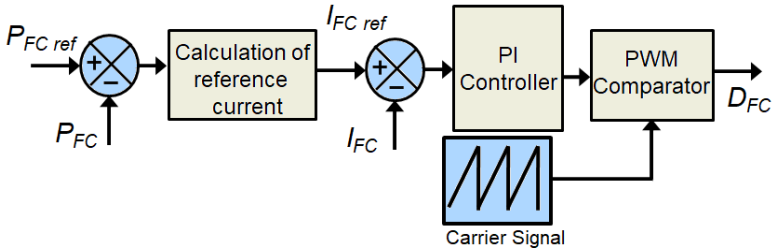

Figure 9. Control strategy for the FCs

4.4 EMS Agent

Because Renewable Energy Sources (RES) are sensitive to environmental factors, their energy production capability might fluctuate with the seasons. Because of this, continuous control approaches cannot be used to satisfy the energy management requirements of an MG. A combination of discrete and continuous control approaches has been included in the multi-agent energy management system under consideration. Controls for each agent's systems are handled by a single unit, the continuous control unit. PV, wind energy systems, and FC agents continually execute local control tasks in the proposed multi-agent control system structure (Khan et al., 2016). In addition, the DC-AC converter continually performs harmonic compensation in the load. An agent of energy management, a discrete controller, is responsible for making decisions about how the MG should operate by gathering data from other agents and sending commands to switches S_{FC1} and S_{FC2}, which then circulate FC_1 and FC_2 while maintaining energy balance and system stability in the face of unpredictable environmental conditions such as switching linear loads. Figure 10 depicts the arrangement of the internal components of this controller. This controller has a total of five different modes. The mode: 1, mode: 2, mode: 3, mode: 4, and mode: 5 indicators display whether the S_{FC1} and S_{FC2} switches are in the closed or open state. When the amount of electricity transferred from the grid to the MG is more than 0.5 kW, the control system operates in mode 1. Within this setting, the location of the switches is (S_{FC1}: ON. S_{FC2}: ON).

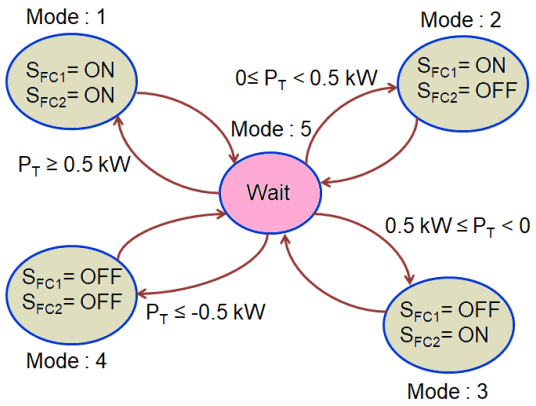

Figure10. Controller for EMS Agent

The control system enters mode: 2 when the amount of power that is transferred from the grid to the MG is lowered to $0 \leq P_T \leq 0.5$kW. The positions of the switches are as follows in mode:2: (S_{FC1}: ON. S_{FC2}: OFF). The mode:3 setting is within the range of $-0.5\text{kW} \leq P_T < 0$, and the switch position is (S_{FC1}: OFF. S_{FC2}: ON). Furthermore, if the P_T value is less than 0.5kW, the control system will switch to mode:4, and the switches will be in position (S_{FC1}: OFF. S_{FC2}: OFF). Within the discrete control structure, the wait mode is denoted by the mode: 5. Because power networks need to wait for a certain amount of time to pass between each change to reach stable conditions, the controller needs to wait for a certain amount of time after applying any change to the working conditions of the MG before it can receive the input data. This is because power networks need to pass a certain amount of time after each change to reach stable conditions.

This controller receives as input the power that is generated by PV, wind energy systems, and FCs, the amount of power that is needed by consumers, and the amount of power that is traded between the MG and the grid. This controller makes decisions on the operational state of the network by collecting the necessary data from other agents in accordance with the various criteria. The condition that must be met to go from one state to another is shown in Figure 10.

5. RESULTS AND DISCUSSION

The performance of the HRES-based STATCOM system is improved by the implementation of the suggested FLC-IPR control scheme, which is based on an auto-tuned PI controller. To validate the effectiveness and functionality of the proposed controller, simulation models are built in the MATLAB/Simulink environment to represent the suggested system and approach. The FLC-IPR control scheme-based auto-tuned PI controller has the advantage of successfully compensating for the current harmonics and reactive power. This is the FLC-IPR controller's primary advantage. The effectiveness of the proposed HRES-based STATCOM is evaluated using both linear and nonlinear loads, in addition to an FLC-based IPR control system, in a range of circumstances.

5.1 Case 1: Varying Load Condition

Figure 11 depicts the performance of the proposed HRES-based STATCOM under the circumstance of abrupt load variation, with the assumption that the balanced supply voltages are in existence. When there is a change in the load, the compensatory current reacts faster to the changes in order to adjust the harmonic current that is present in the load, as seen in Figure 11 (c). Figure 12 illustrates the voltage of the PV array.

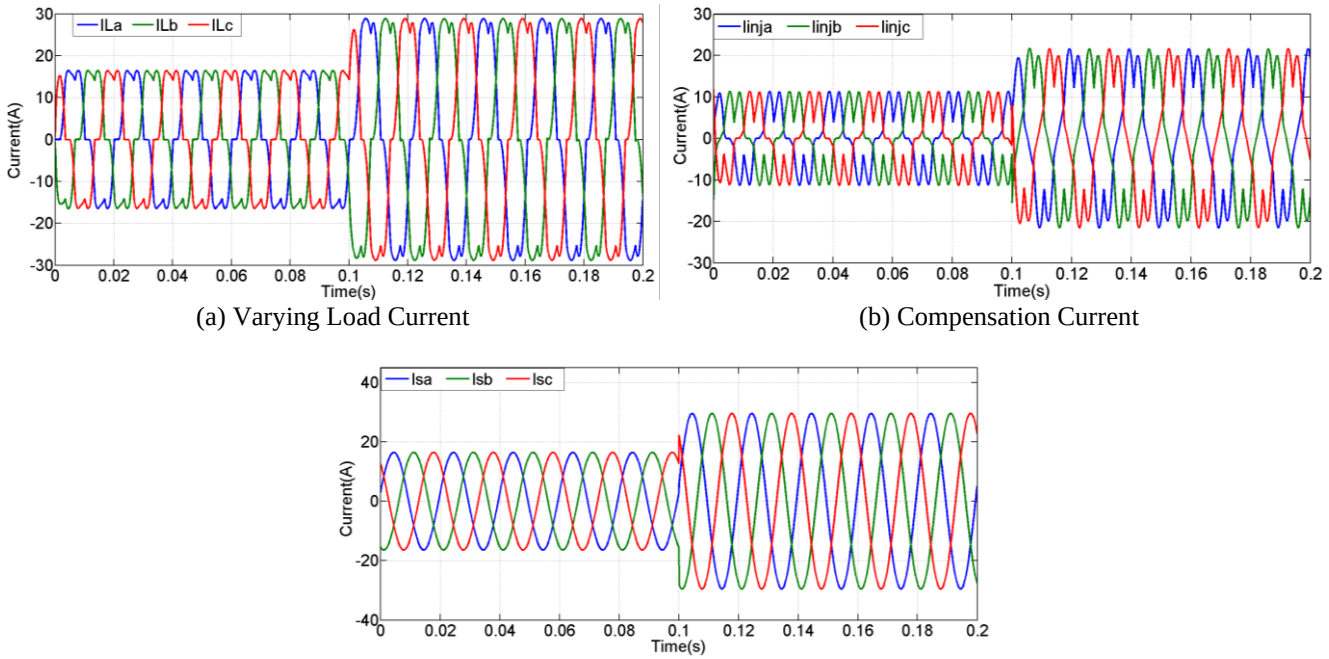

(a) Varying Load Current

(b) Compensation Current

(c) Source Current with Compensation

Figure 11. (a) Varying load current; (b) Compensation current; (c) Source current with compensation

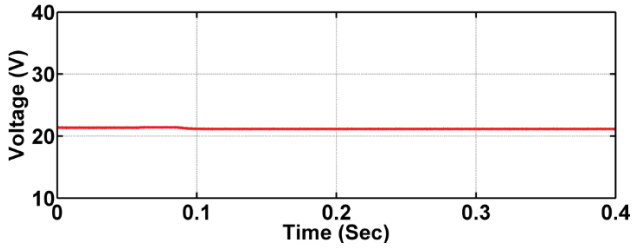

Figure 12. PV Array Voltage

It has been observed that the HRES-based STATCOM that utilizes the suggested technique achieves superior performance than that of the traditional system. As shown in Fig. 13, the Total Harmonic Distortion (THD) of the source current may be efficiently decreased from 24.10(%) to 1.26(%), depending on which approach is used. As a result, this transient occurrence reveals the real capabilities of the suggested technique and enhances its performance in comparison to the present approach. The proportion of THD in the current can be shown to decrease following adjustment in Figure 13(b). With the assistance of the FLC-IPR control system, the total harmonic distortion of the source current is shown to decrease, which satisfies the criteria outlined in the IEEE-519 standard.

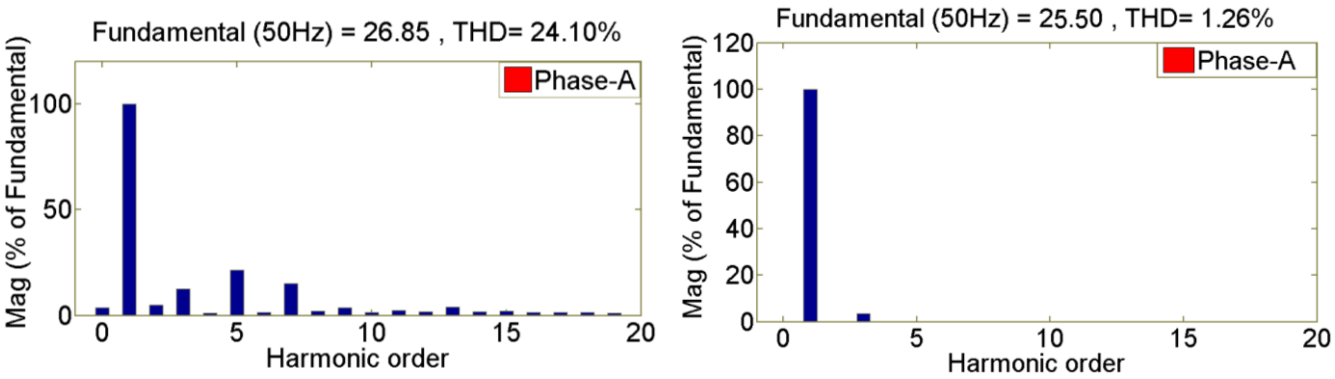

(a) Load Current Harmonics (b) Source Current Harmonics with Compensation

Figure 13. Harmonics analysis: (a) Load current harmonics (b) Source current harmonics with compensation

To test the effectiveness of the suggested controller that is based on the FLC-IPR control algorithm, an experimental prototype of the configuration that has been presented has been developed in the laboratory. The solar photovoltaic (PV) system is linked to the DC connection of the STATCOM module. The experimental prototype that was developed using the dSPACE 1103 controller has been chosen to establish the control algorithm that will generate switching signals for the SEMIKRON IGBT module, which is considered to be STATCOM in this application. The Hall effect voltage and current transducers have been providing the signal as well as the logic that has been necessary for real-time data collecting. To validate the proposed controller that is based on the FLC-IPR control algorithm, a real-time controller has been developed into a dSPACE 1103 compatible environment via the use of the host computer. STATCOM is responsible for eliminating harmonics that may be present in the current to get a sinusoidal source current. The existence of harmonics in the load current as a result of nonlinear loads that do not have compensation is shown in Figure 14 (a). However, the FLC-IPR control method can provide a smoother source current by using the PI gains at their ideal levels. The FLC-IPR control technique is shown alongside the three-phase source current in Figure 14(b).

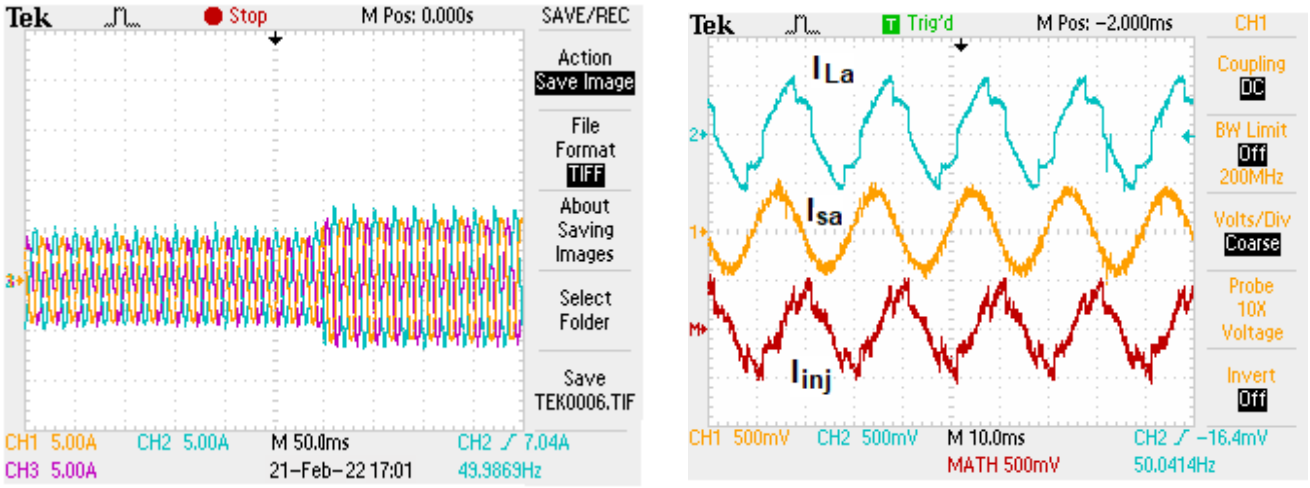

(a) Varying Load Current (b) Load, Source and Injected Current

Figure 14. (a) Varying load current (b) Load, source and injected current

Before compensation is applied, the THD of the load currents is 24.3%. As can be seen in Figure 15(b), the THD value is brought down to 1.2 % after the FLC-IPR control technique has been applied. The DC link voltage and PV array voltage are shown in Figure 16.

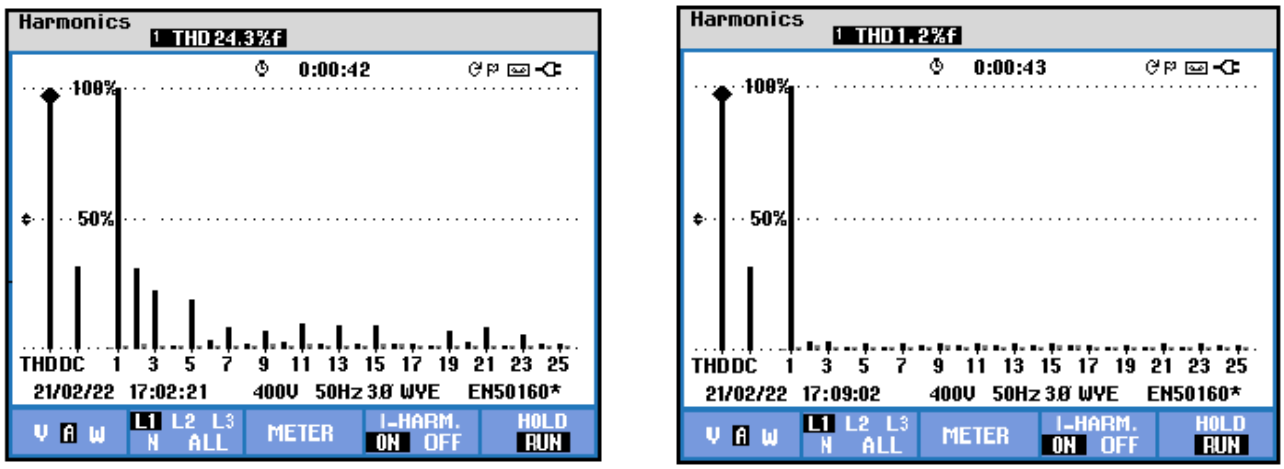

(a) THD before Compensation is Applied (b) THD before Compensation is Applied

Figure 15. THD level before and after compensation applied

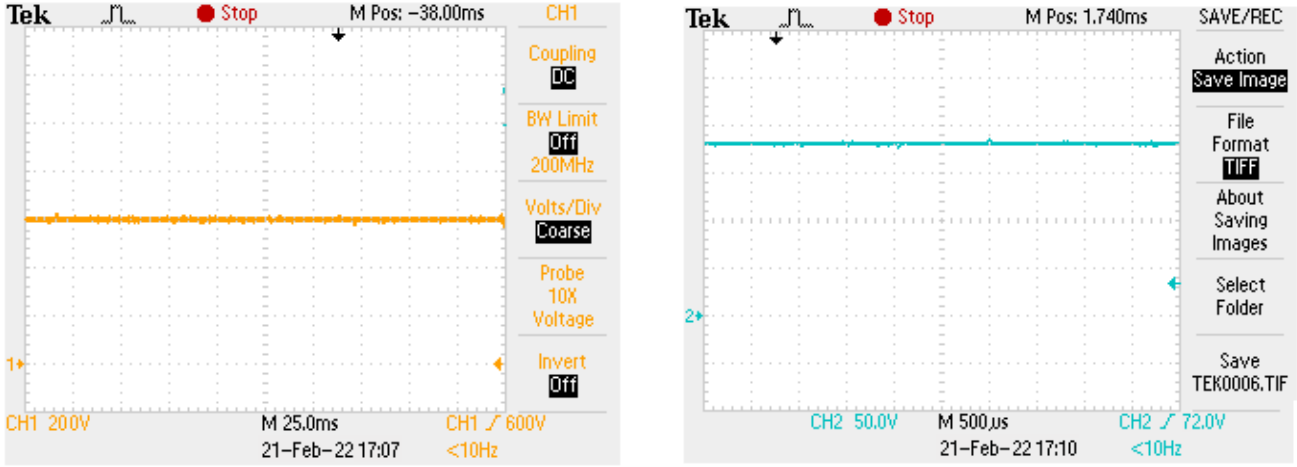

(a) DC-link voltage (b) PV Array Voltage

Figure 16. DC link voltage and PV array voltage

5.2 Case 2: Varying Wind Speed

Figure 17 depicts the performance of the controller under different wind speeds while maintaining the same amount of applied consumer load. At 0.04 seconds, when the wind speed goes from 7m/s to 10m/s, the generator current goes up. As a result, the load at which the generator is being used experiences a reduction in the current that is being supplied by the other renewable energy source. This is because the generator is now able to meet the load demand, and there is sufficient wind power available. After a delay of 0.08 seconds, the wind speed drops from 10 m/s to 9 m/s, and it is then noted that other renewable sources begin producing electricity to fulfill the demand of consumer loads. In this way, the controller may offer load leveling and control of the frequency at which the voltage is produced.

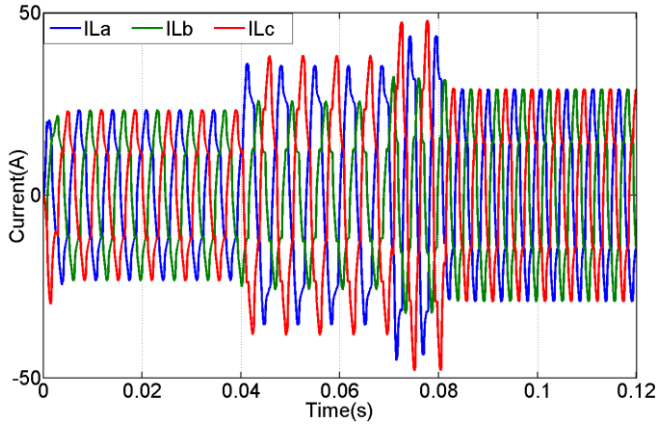

(a) Load Current

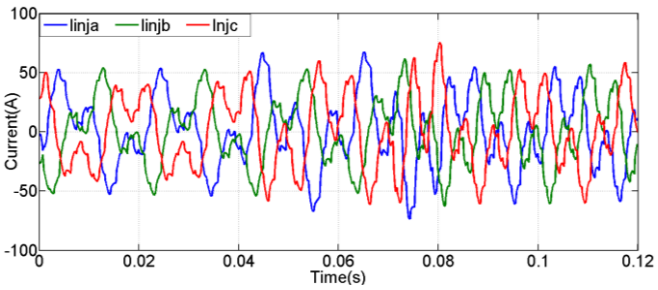

(b) Injected Voltage

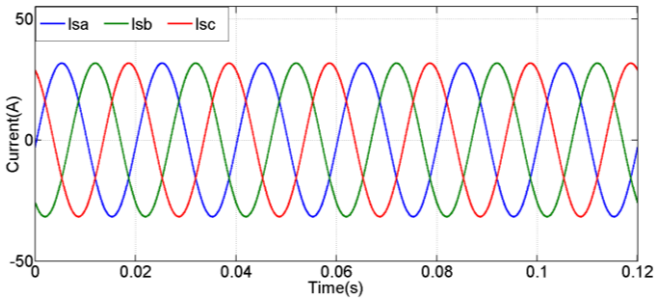

(c) Source voltage

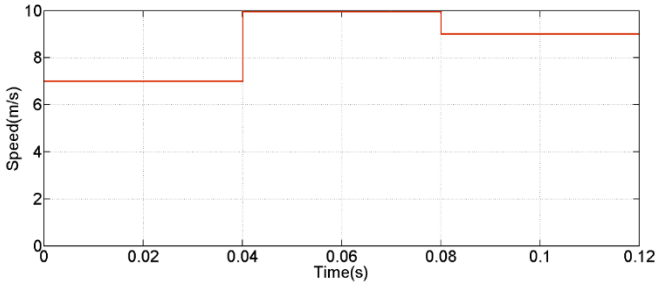

(d) Varying Wind Speed

Figure 17. performance of the controller under different wind speeds: (a) Load current; (b) Injected voltage; (c) Source current; (d) Varying wind speed

Before compensation is applied, the THD of the load currents is 25.15%. As can be seen in Figure 18(b), the THD value is brought down to 1.24% after implementing HRES-based STATCOM with the FLC-IPR control technique.

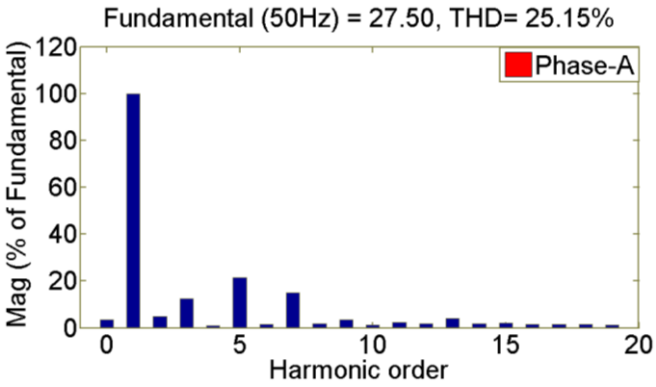

(a) Load Current Harmonics

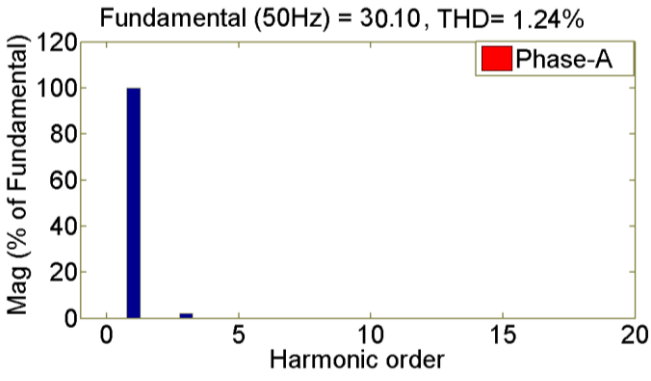

(b) Source Current Harmonics with Compensation

Figure 18. Harmonics analysis: (a) Load current harmonics (b) Source current harmonics with compensation

To get a sinusoidal source current, it is the responsibility of STATCOM to remove any harmonics that may be present in the current. Figure 19(a) illustrates the presence of harmonics in the load current as a direct consequence of nonlinear loads that do not have compensation. The source current with compensation applied is shown in Figure 19(b).

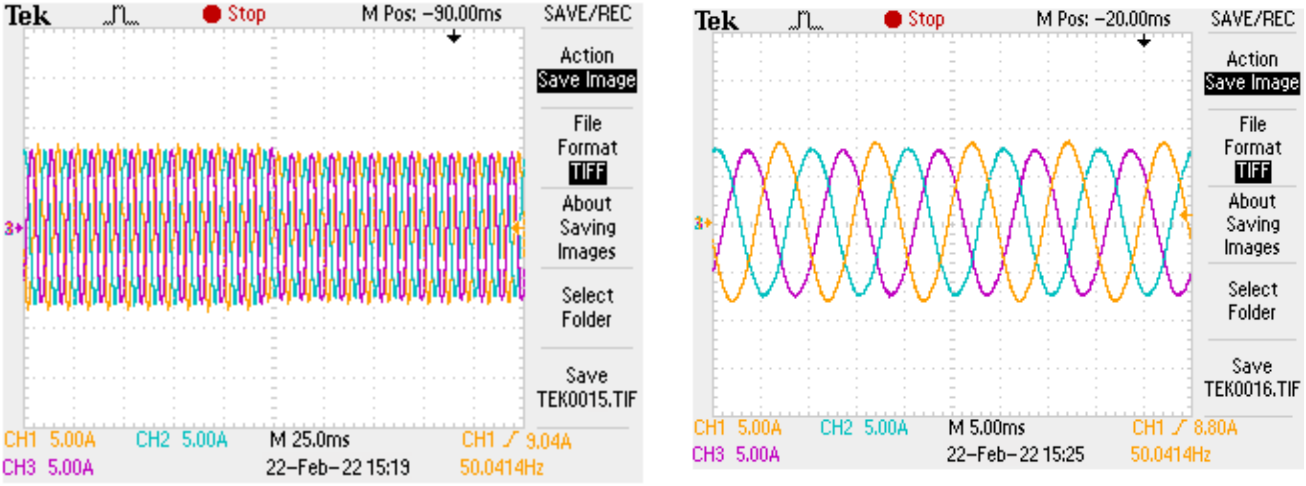

(a) Load Current (b) Source Current with Compensation Applied

Figure 19. Results of experimentation: (a) Load current (b) Source current with compensation applied

Before compensation is applied, the THD of the load currents is 25.2%. As can be seen in Figure 20(b), the THD value is brought down to 1.2 % after implementing the HRES-based STATCOM with the FLC-IPR control technique. The DC link voltage, source voltage, and current are shown in Figure 21.

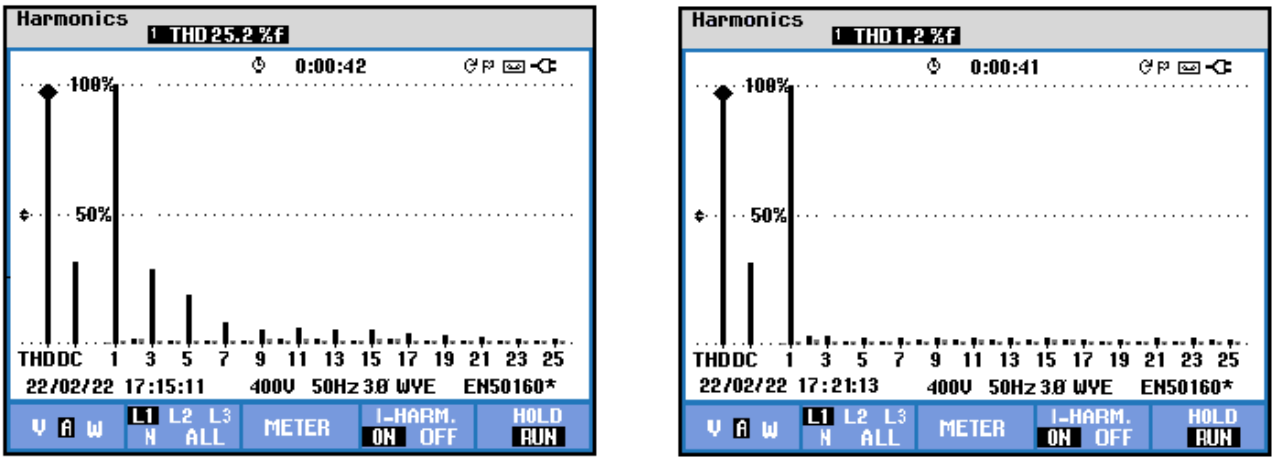

(a) Load Current THD before Compensation Applied (b) Load Current THD after Compensation Applied

Figure 20. THD level before and after compensation applied

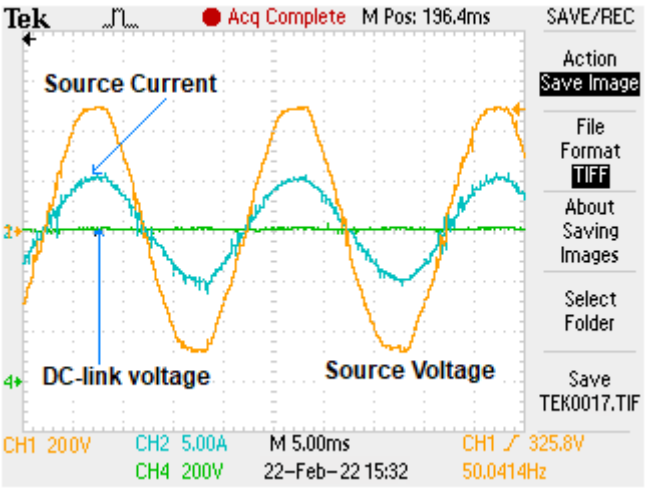

Figure 21. DC Link Voltage, Source Voltage and Current

5.3 Case 3: Varying Solar Irradiation

Figure 22 depicts the performance of the proposed HRES-based STATCOM under the circumstance of varying solar irradiation, with the assumption that the balanced supply voltages are in existence. When there is a harmonic distortion in the load current, the compensatory current reacts faster to the changes to adjust the harmonic current that is present in the load, as seen in Figure 22.

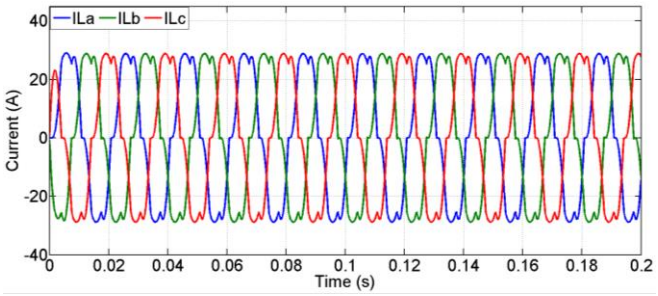

(a) Load Current

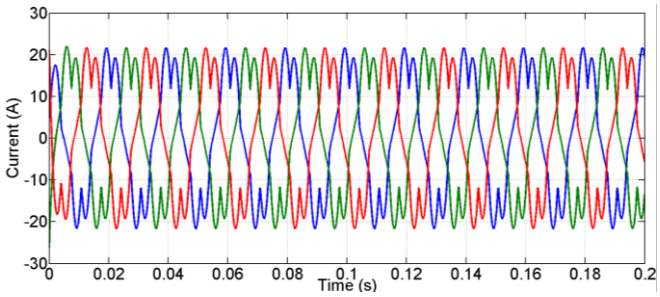

(b) STATCOM Injected Current

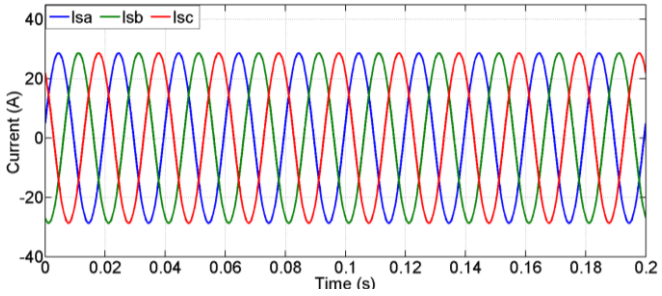

(c) Source Current with Compensation Applied

Figure 22. Current compensation results: (a) Load current; (b) STATCOM injected current; (c) Source current with compensation applied

Figure 23(a), it is revealed that an increase in irradiation conditions from 500 W/m^2 to 1000 W/m^2 helps increase the PV array voltage.

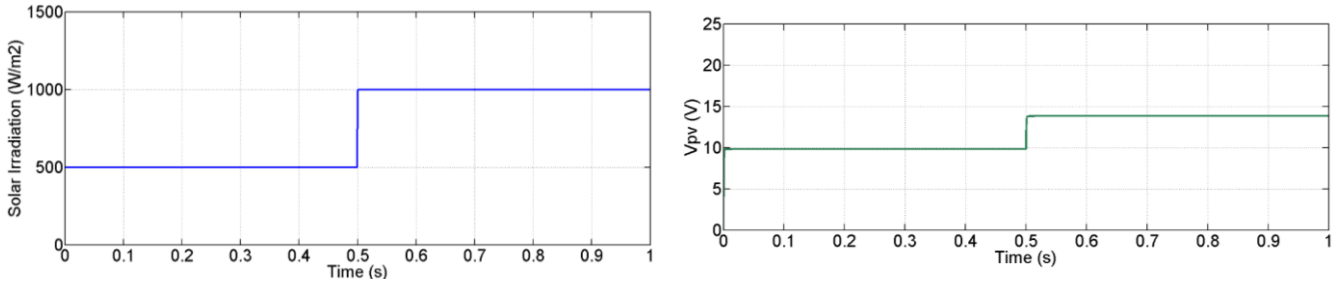

(a) Varying Solar Irradiation (b) PV Array Voltage with Varying Solar Irradiation

Figure 23. (a) Varying solar irradiation (b) PV array voltage with varying solar irradiation

The THD of the load currents is 24.63% before any compensation is implemented. After adopting the HRES-based STATCOM with the FLC-IPR control approach, the THD value was decreased to 1.24%, as shown in Figure 24(b), which shows that the reduction was successful.

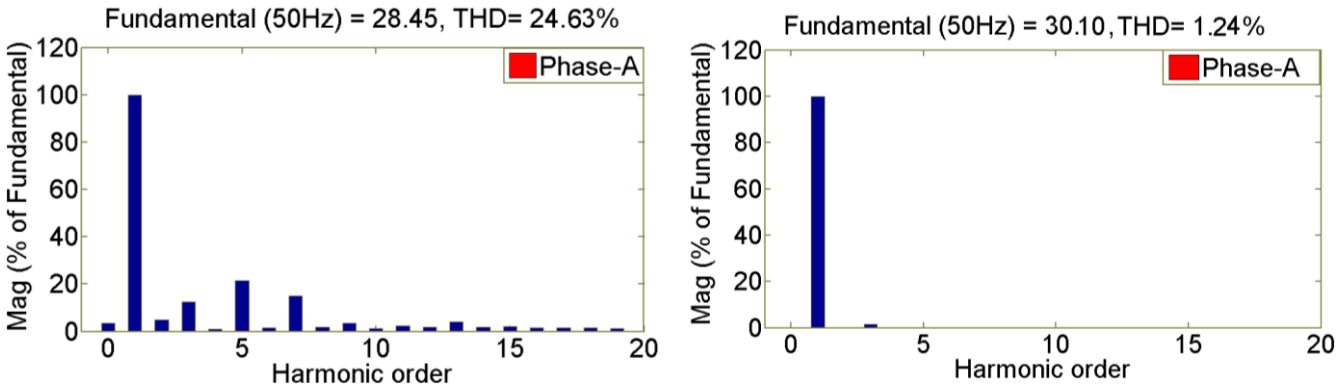

(a) Load Current Harmonics (b) Source Current Harmonics with Compensation

Figure 24. Harmonic analysis: (a) Load current harmonics (b) Source current harmonics with compensation

Power-sharing between different power sources, such as wind energy and Fuel cell and load power, is shown in Figure 25.

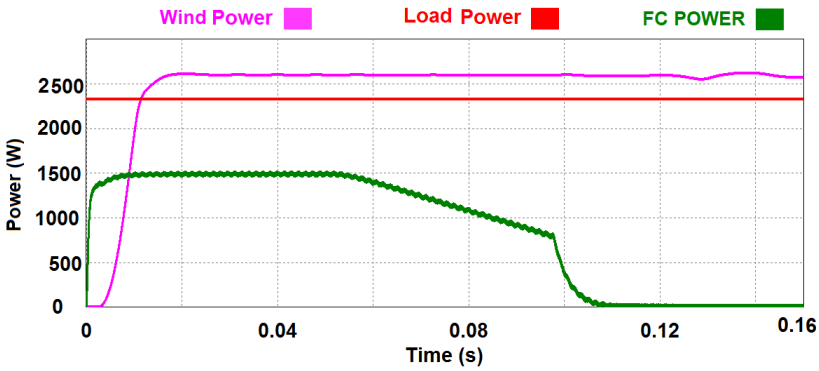

Figure 25. Power Sharing between Different Sources

STATCOM is capable of removing any harmonics that could be present in the current to provide a sinusoidal supply current. Fig. 26(a) shows the presence of harmonics in the load current as a consequence of nonlinear loads that do not have compensation. Fig. 26(b) shows the sinusoidal supply current with compensation applied.

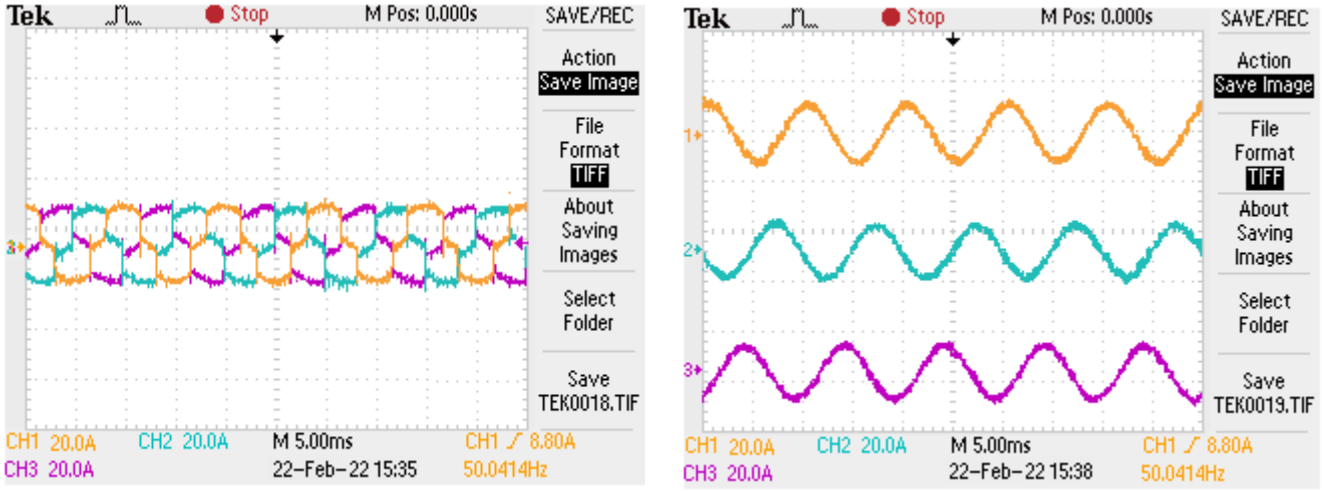

(a) Load Current (b) Sinusoidal Supply Current with Compensation Applied

Figure 26. Current compensation experimental results: (a) Load current (b) Sinusoidal supply current with compensation applied

It is visible from Figure 27 that decreasing the irradiation from 1000 W/m2 to 500 W/m2 reduces the source current. While the load current THD level is 25.2% before compensation is applied in phase "*a*," as shown in Figure 28(a). Three-phase source currents are balanced and sinusoidal after compensation with the proposed method, and the THD level of source current after compensation is applied at 1.2% in phase "*a*," as shown in Figure 25(b).

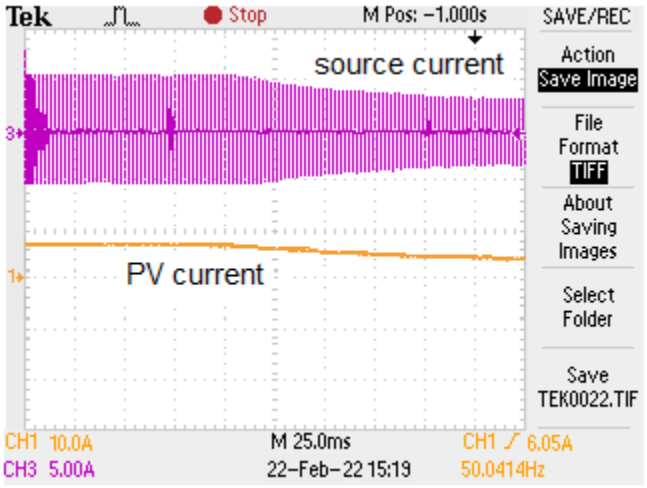

Figure 27. PV-STATCOM Performance under Irradiation Variations.

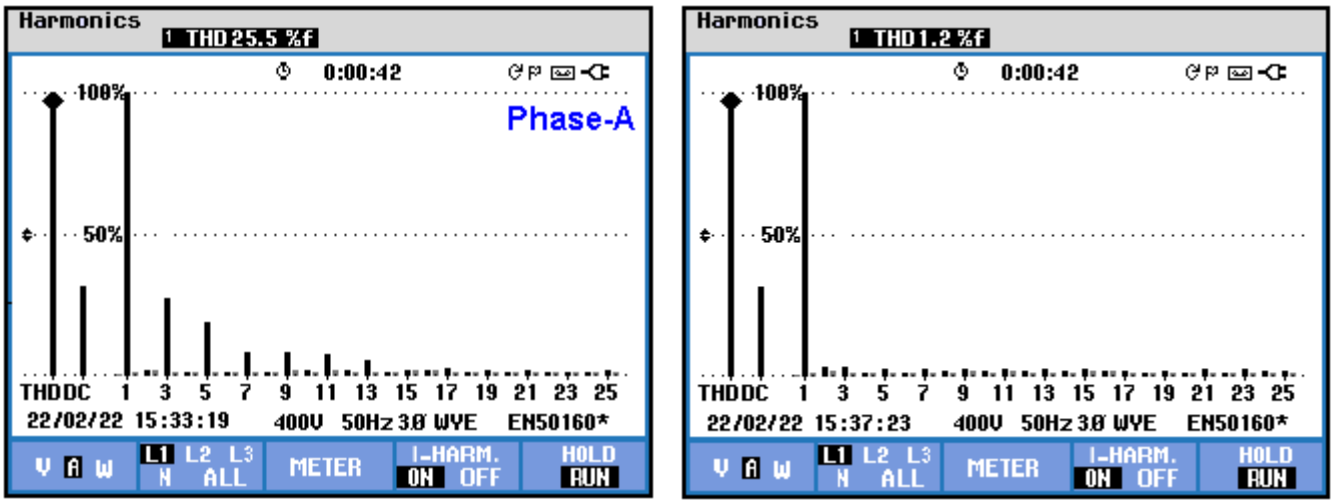

(a) Load Current THD Level before Compensation Applied

(b) THD Level of Source Current after Compensation Applied

Figure 28. (a) Load current THD level before compensation applied (b) THD level of source current after compensation applied

Table 2 illustrates that the percentage of THD in the current is being reduced mostly after compensation under the simulation study. It is evident that the THD of the source current decreases with the help of the FLC-IPR controller and fulfills the requirement of the IEEE-519 standard.

Table 2. Harmonic spectrum of source current after compensation with FLC-IPR controller under simulation study

Phases	**Load Current THD (%)**			**Source Current THD (%) with FLC-IPR Control**		
	Case: 1	**Case: 2**	**Case: 3**	**Case: 1**	**Case: 2**	**Case: 3**
A-Phase	24.10	25.15	24.63	1.26	1.24	1.24
B-Phase	24.30	25.22	24.60	1.25	1.25	1.25
C-Phase	24.50	25.30	24.55	1.26	1.25	1.23

In the following experimental study, Table 3 displays the harmonic spectrum of the source current both before and after correction using the FLC-IPR controller.

Table 3. Harmonic spectrum of source current after compensation with FLC-IPR controller under experimental study

Phases	**Load Current THD (%)**			**Source Current THD (%) with FLC-IPR Control**		
	Case: 1	**Case: 2**	**Case: 3**	**Case: 1**	**Case: 2**	**Case: 3**
A-Phase	24.3	25.2	25.5	1.2	1.2	1.2
B-Phase	24.4	25.3	25.6	1.2	1.2	1.2
C-Phase	24.4	25.4	25.6	1.2	1.3	1.2

In the suggested technique, the current harmonics THD level is extremely low, approximately 1.2%, when compared to the conventional methods, which have a load current THD of 3.4%, as stated by Gupta (2022). This is the case even when the load circumstances are nonlinear. It can be observed that the source currents are smooth and have less distortion in the case of the suggested methodology in comparison to the way that is already being used. Therefore, the suggested technique provides a higher level of effective compensation for harmonics. In the case of the suggested technique, the THD response of the source current after compensation is better than in the case of the existing method.

6. CONCLUSION

In this study, a novel energy management technique is proposed to regulate active and reactive power in an MG consisting of many DER, namely PV, WT, and FC, and a set of loads that comprises changeable linear and non-linear loads. The energy of the DG is managed by a structure made up of several agents that implement the method that has been suggested. Three different agents were presented in the MAS, and each of these agents represented a different component of the MG. The MATLAB/Simulink Simpower systems environment was used for the development and simulation of each component and agent model that makes up the MG. The MPPT controller is installed in both the PV and WT agents so that they can gather the most possible energy. The energy management unit receives the measured parameters that are connected to the required load as well as the energies that are exchanged between the microgrid and the grid from the load and grid agents. The energy management unit comes to a suitable conclusion on the quantity of energy that will be generated by two FCs after considering both the energy strategy and the information that was obtained from other agents. Due to the high cost of the energy generated by FCs, an effort was made to bring down the overall cost of energy in the microgrid by managing the FCs. A STATCOM is also used for the current harmonic compensation of a non-linear load. The results of the simulation reveal that the established strategy for energy management performs effectively in reaching the objectives of reducing the cost of energy while simultaneously enhancing the degree of independence experienced by the microgrid and providing harmonic compensation.

REFERENCES

Ambia, M.N., Al-Durra, A., Caruana, C., and Muyeen, S.M. (2014). Power Management of Hybrid Microgrid System by A Generic Centralized Supervisory Control Scheme. *Sustainable Energy Technologies and Assessments*, 8: 57-65. DOI: 10.1016/j.seta.2014.07.003.

Benlahbib, B., Bouarroudj, N., Mekhilef, S., Abdeldjalil, D., Abdelkrim, T., Bouchafaa, F., and lakhdari, A. (2020). Experimental Investigation of Power Management and Control of PV/Wind/Fuel Cell/Battery Hybrid Energy System Microgrid. *International Journal of Hydrogen Energy*, 45(53): 29110-29122.

Chauhan, R. K., Hasan, M., and Pandey, J. P. (2018). Intelligent Control Model to Enhance The Performance of Unified Power Quality Conditioner. *Journal of Intelligent & Fuzzy Systems*, 35(5): 5007-5020.

Dash, V. and Bajpai, P. (2015). Power Management Control Strategy for A Stand-Alone Solar Photovoltaic Fuel Cell–Battery Hybrid System. *Sustainable Energy Technologies and Assessments*, 9:68-80. DOI: 10.1016/j.seta.2014.10.001.

Delgoshaei, A., Mohammadazari, M., Hanjani, S.E., Fard, F., Beigizadeh, R., and Aram, A.K. (2021). A Fuzzy Logic-Based Algorithm for Supply Chain Management Considering Different Cases. *International Journal of Industrial Engineering: Theory, Applications, and Practice*, 27(6). DOI: Https://doi.org/10.23055/Ijietap.2020.27.6.5883.

Dou, C. X., Wang, W. Q., Hao, D. W., and Li, X. B. (2015). MAS-Based Solution to Energy Management Strategy of Distributed Generation System. *Int J Electr Power Energy Syst*., 69: 354–366.

Elgamal, M., Korovkin, N., Elmitwally, A., Chen, Z. (2020). Robust Multiagent System for Efficient Online Energy Management and Security Enforcement in a Grid-Connected Microgrid with Hybrid Resources. *IET Generation, Transmission & Distribution*, 14(9): 1726-1737. DOI: 10.1049/iet-gtd.2019.1284.

Gupta, S. (2022). Power Quality Evaluation of Photovoltaic Grid Interfaced Cascaded H-Bridge Nine-Level Multilevel Inverter Systems Using D-STATCOM and UPQC. *Energy*, 238: 121707.

IEEE Recommended Practice and Requirements for Harmonic Control in Electric Power System, IEEE Std 519-2014 (Revision of IEEE Std 519-1992), 1-29. DOI: 10.1109/IEEESTD.2014.6826459.

Karavas, C. S., Kyriakarakos, G., Arvanitis, K.G, and Papadakis, G. (2015). A Multi-Agent Decentralized Energy Management System Based on Distributed Intelligence for the Design and Control of Autonomous Polygeneration Microgrids, *Energy Conversion Management*, 103: 166-179. DOI:10.1016/j.enconman.2015.06.021

Khan, M. R. B., Jidin, R., and Pasupuleti, J. (2016). Multi-Agent Based Distributed Control Architecture for Microgrid Energy Management and Optimization. *Energy Conversion and Management*, 112: 288-307.

Mohammed, A., Refaat, S. S., Bayhan, S., and Abu-Rub, H. (2019). AC Microgrid Control and Management Strategies: Evaluation and Review. *IEEE Power Electronics Magazine*, 6(2): 18-31.

Muduli, U. R. and Ragavan, K. (2014). Dynamic Modeling and Control of Shunt Active Power Filter. 2014 *Eighteenth National Power Systems Conference (NPSC)*, Guwahati, India, 1-6. DOI: 10.1109/NPSC.2014.7103893.

Muthuvel, K. and Vijayakumar, M. (2020). Solar PV Sustained Quasi Z-Source Network-Based Unified Power Quality Conditioner for Enhancement of Power Quality. *Energies*, 13(10): 2657.

Ngamroo, I. (2012). Application of Electrolyzer to Alleviate Power Fluctuation in A Stand-Alone Microgrid Based on An Optimal Fuzzy PID Control. *International Journal Electric Power Energy System*, 43(1): 969-976. DOI: 10.1016/j.ijepes.2012.05.051.

Parthiban, S. and Vijayakumar, M. (2021). Experimental Validation of Solar PV Sustained ZSI Based Unified Active Power Filter for Enrichment of Power Quality. *Automatika*, 62(1): 137-153.

Prasad, D., Kumar, N., and Sharma, R. (2022). Grid Interfaced Solar-Wind Hybrid Power Generating Systems Using Fuzzy-Based TOGI Control Technique for Power Quality Improvement. *Journal of Intelligent & Fuzzy Systems*, 42(2): 1127-1139.

Prince, S., Panda, K., and Panda, G. (2019). Kalman Filter Variant Intelligent Control for Power Quality Improvement in Photovoltaic Active Power Filter System. *International Transactions on Electrical Energy Systems*. 30(3): 1-22, doi:10.1002/2050-7038.12239.

Rahmani-Andebili, M. (2017). Stochastic, Adaptive, and Dynamic Control of Energy Storage Systems Integrated with Renewable Energy Sources for Power Loss Minimization. *Renew Energy*, 113: 1462-1471, DOI: 10.1016/J.Renene.2017.07.005.

Raja, A, Vijayakumar, M., and Karthikeyan, C. (2022). Solar Photovoltaic Interconnected ZSI-Unified Power Quality Conditioner to Enhance Power Quality. *Bulletin of The Polish Academy of Sciences Technical Sciences*, 70(1): 1-10.

Rajesh, K. S., Dash, S. S., Rajagopal, R., and Sridhar, R. (2017). A Review on Control of AC Microgrid. *Renewable and Sustainable Energy Reviews*, 71: 814-819.

Shahgholian, G. (2021). A Brief Review on Microgrids: Operation, Applications, Modeling, and Control. *International Transactions on Electrical Energy Systems*, 31(6): 1-28.

Talapur G, Suryawanshi, H/, Xu, L., Shitole, A. (2018). A Reliable Microgrid with Seamless Transition Between Grid Connected and Islanded Mode for Residential Community with Enhanced Power Quality. *IEEE Trans Ind Appl*., 54(5): 5246-5255. DOI: 10.1109/Tia.2018.2808482.

Toghani Holari, Y., Taher, S. A., and Mehrasa, M. (2020). Distributed Energy Storage System Based Nonlinear Control Strategy for Hybrid Microgrid Power Management Included Wind/PV Units in Grid Connected Operation. *International Transactions on Electrical Energy Systems*, 30(2): 1-20.

Torreglosa, J., García, P., Fernández, L., and Jurado, F. (2015). Energy Dispatching Based on Predictive Controller of An Off-Grid Wind Turbine/Photovoltaic/Hydrogen/Battery Hybrid System. *Renew Energy*, 74: 326-336. DOI: 10.1016/J.Renene.2014.08.010.

Tseng, B., Rosales, C., and Kwon, Y. (2014). Optimization of Wind Turbine Placement Layout on Non-Flat Terrains. *International Journal of Industrial Engineering: Theory, Applications, and Practice*, 21(6). DOI: Https://doi.org/10.23055/ijietap.2014.21.6.1265.

Vijayakumar, M. and Vijayan, S. (2014). PV Based Three-Level NPC Shunt Active Power Filter with Extended Reference Current Generation Method. *International Journal of Electrical Energy*, 2(4): 258 – 267.

Wang, R., Wang, P., Xiao, G., and Gong, S. (2014). Power Demand and Supply Management in Microgrids with Uncertainties of Renewable Energies. *Int J Electr Power Energy Syst*., 63: 260–269.

Wang, T., O'Neill, D., and Kamath, H. (2015). Dynamic Control and Optimization of Distributed Energy Resources in A Microgrid. *IEEE Transactions on Smart Grid*, 6(6): 2884-2894. DOI: 10.1109/TSG.2015.2430286.

Xu, X., Jia, H., Wang, D., Yu, D.C., and Chiang, H.D. (2015). Hierarchical Energy Management System for Multi-Source Multi-Product Microgrids. *Renewable Energy*, 78: 621-630. DOI:10.1016/j.renene.2015.01.039

Zeng, Z., Yang, H., Zhao, R., and Cheng, C. (2013). Topologies and Control Strategies of Multi-Functional Grid-Connected Inverters for Power Quality Enhancement: A Comprehensive Review. *Renewable and Sustainable Energy Reviews*, 24: 223-270. DOI: 10.1016/J.Rser.2013.03.033.

APPENDIX

System Phase voltage = 230V, Frequency (*f*) =50Hz, STATCOM parameters: V_{dc} = 600V, L_f= 26 mH, R_f =1.5Ω, Switching frequency= 10kHz, PV array Power=250W,V_{OC}=23.9V, I_{mpp} =12.38A, WECS parameters: V_L=400V, P=5kW, Rated Rotor speed (*N*)= 1410 rpm, Fuel Cell parameters: Rated power=1.7kW, efficiency=70%, Load parameters: Three-phase thyristor rectifier: 3mH,5.7mH,12Ω, RL load : 7Ω,75mH.